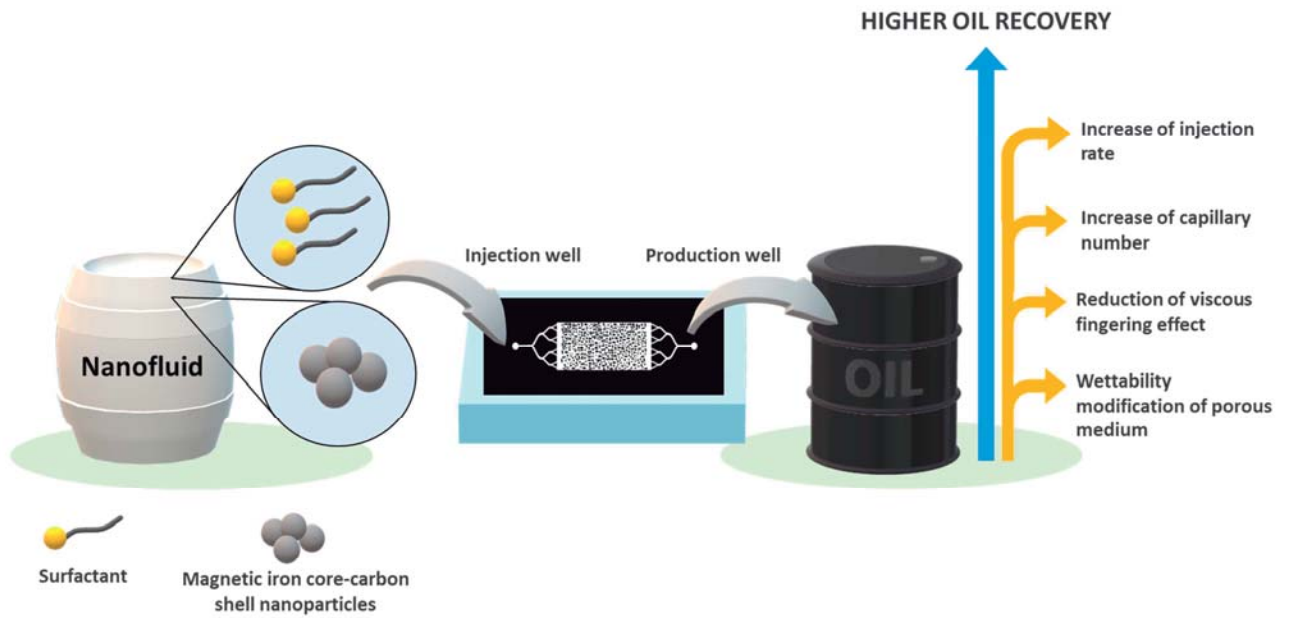


GRAPHICAL ABSTRACT



Journal

A Microfluidic Study to Investigate the Effect of Magnetic Iron Core-Carbon Shell Nanoparticles on Displacement Mechanisms of Crude Oil for Chemical Enhanced Oil Recovery

Stefanía Betancur^{1,4,*}, Carol M. Olmos^{1,2}, Maximiliano Pérez^{2,3,*}, Betiana Lerner^{2,3}, Camilo A. Franco¹, Masoud Riazi⁵, Jaime Gallego^{1,6}, Francisco Carrasco-Marín⁴, Farid B. Cortés¹

¹ Grupo de Investigación en Fenómenos de Superficie – Michael Polanyi, Facultad de Minas, Universidad Nacional de Colombia Sede Medellín, Cra 80 No. 65-223, 050034, Medellín, Colombia.

² Universidad Tecnológica Nacional (UTN), Facultad Regional Haedo, Haedo, Buenos Aires, Argentina, E 1706.

³ Universidad de Buenos Aires (UBA), Facultad de Ingeniería, Instituto de Ingeniería Biomédica, Buenos Aires, Argentina, C1063ACV.

⁴ Grupo de Investigación en Materiales de Carbón, Departamento de Química Inorgánica, Facultad de Ciencias, Universidad de Granada, 18071, Granada, Spain.

⁵ Department of Petroleum Engineering, School of Chemical and Petroleum Engineering, Shiraz University, Shiraz, Iran.

⁶ Química de Recursos Energéticos y Medio Ambiente, Instituto de Química, Universidad de Antioquia UdeA, Calle 70 No. 52-21, 050010, Medellín, Colombia.

* Corresponding author: sbetancurm@unal.edu.co, mperez@frh.utn.edu.ar

ABSTRACT

The main objective of this work is to evaluate the effect of the simultaneous use of a surfactant mixture and magnetic iron core-carbon shell nanoparticles on oil recovery via a microfluidic study based on the rock-on-a-chip technology. The surfactant solution used for all experiments was prepared based on a field formulation and consisted of a mixture of a hydrophilic and a lipophilic surfactant. Magnetic iron core-carbon shell nanoparticles with a mean particle size of 60 nm and a surface area of $123 \text{ m}^2 \cdot \text{g}^{-1}$ were employed. The displacement experiments consisted of waterflooding, surfactant flooding and nanoparticle-surfactant flooding and were performed using PDMS (polydimethylsiloxane)-glass microdevices type random network. The characteristics and design of the microfluidic device allowed to emulate a mixed wettability of a porous medium. Then, the oil was displaced by injecting the solution at a constant injection rate, until steady-state conditions were obtained. Furthermore, the effect of three injection rates corresponding to $0.1 \text{ ft} \cdot \text{day}^{-1}$, $1 \text{ ft} \cdot \text{day}^{-1}$, and $10 \text{ ft} \cdot \text{day}^{-1}$ was investigated. The increase in the injection rate favored the oil recovery percentage. In addition, for all injection rates, the oil recovery decreased in the following order: nanoparticle-surfactant flooding > surfactant flooding > waterflooding. The nanoparticle-surfactant system at the injection rate of $1.9 \mu\text{L} \cdot \text{min}^{-1}$ presented the highest oil recovery (i.e., 84%). Likewise, nanoparticle-surfactant flooding showed a more stable displacement front and consequently, the highest capillary number among the injection fluids. Oil recovery by waterflooding was the lowest among the evaluated systems due to the viscous fingering phenomena under different injection rates. In addition, it can be observed that for all injection rates, the presence of the surfactant mixture and nanoparticles reduce the

viscous fingering effect. The results can be used to visually and quantitatively analyze the role of the simultaneous use of nanoparticles with surfactants in enhanced oil recovery processes.

KEYWORDS: Microfluidic; enhanced oil recovery; nanoparticles; surfactant.

1. INTRODUCTION

Chemical enhanced oil recovery (CEOR) refers to the injection of fluids and chemicals into a reservoir to modify the rock/oil/brine interactions in order to increase oil recovery (Alvarado and Manrique, 2010; Sheng, 2010). CEOR methods include the addition of chemical agents to increase areal and vertical sweep efficiency and also pore-scale displacement efficiency of crude oil (Muggeridge et al., 2014). These chemicals should lead to cost-effective operations to be considered as an option for developing matured fields in times of the low price of crude oil barrel (Afolabi, 2015).

The purpose of CEOR is to increase the capillary number, which consists of the ratio between the viscous forces and capillary forces (Salager, 2005). For increasing the capillary number and consequently, the oil recovery percentage, there are four possibilities: to increase the flow rate of injection fluid, to increase the viscosity of the injection fluid, to reduce the interfacial tension (IFT) between the crude oil and injection fluid, and/or the alteration of the porous medium wettability. Specifically, surfactant injection has been employed to impact the last two mechanisms (Jang and Chon, 2014; Kargozarfard et al., 2019; Moslemizadeh et al., 2016).

However, in some EOR processes water fingers through the oil phase may occur (Mai and Kantzas, 2009), which affects sweep efficiency and consequently, oil recovery percentage.

Hence, the use of nanotechnology in chemical enhanced oil recovery processes has increased due to its high impact in the reduction of the interfacial tension (IFT) between crude oil and water (Moghadam et al., 2015; Zargartalebi et al., 2014; Zargartalebi et al., 2015), the alteration of wettability of porous medium (Ehtesabi et al., 2013; Kazemzadeh et al., 2019; Li et al., 2015), the increase in viscosity of injection fluid, and a possible modification of flow pattern (Bennetzen and Mogensen, 2014; Kazemzadeh et al., 2019). Nanoparticles can be modified by adjusting their particle size, surface area, chemical reactivity, catalytic capacity, among others (Christian et al., 2008). Among the different nanoparticles that have been employed, magnetic iron core-carbon shell nanoparticles have been used due to their double functionality (Bennetzen and Mogensen, 2014): the core determines the magnetic properties and the possibility to recover and re-use the nanoparticles in a subsequent EOR process and the shell determines the binding affinity with the surfactant (Betancur et al., 2019a). The magnetic iron core-carbon shell nanoparticles showed a high thermal stability at reservoir conditions, which indicated that the use of these nanoparticles does not cause formation damage problems as it can be observed from the pressure drop curves in the displacement tests carried out by Betancur et al. (Betancur et al., 2019a). Also, the simultaneous use of magnetic iron core-carbon shell nanoparticles and a surfactant mixture achieved to reduce the IFT to the ultralow value of $1 \times 10^{-4} \text{ mN} \cdot \text{m}^{-1}$ ($1 \times 10^{-7} \text{ N} \cdot \text{m}^{-1}$) at a nanoparticle concentration of $100 \text{ mg} \cdot \text{L}^{-1}$. In addition, a final oil recovery of 98% was obtained (Betancur et al., 2019a).

Although the good results that have been obtained with the use of iron core-carbon shell nanoparticles including high recovery percentage in displacement tests under reservoir

conditions, the EOR mechanisms are not fully understood yet. Consequently, the use of nanoparticles combined with conventional chemicals used in EOR has been the focus of several investigations using microfluidic devices to facilitate a better understanding of the displacement of two or more fluids in a porous medium at a laboratory scale (He and Xu, 2016).

Microfluidic devices are a good alternative for flooding tests because of their small size and the reduction of time of calculations, which can take days through conventional laboratory tests (Gogoi and Gogoi, 2019). These features make microfluidic devices a cost-effective alternative to choose a particular treatment before to be tested in field level. For instance, several researchers have focused their work in the use of microfluidic for determining the effect of different chemicals in emulsion behavior and modification of rock wettability (Baret et al., 2009; Kenzhekhanov, 2016; Maurya et al., 2018; Meybodi et al., 2011; Mohajeri et al., 2015; Priest et al., 2011; Romero-Zeron et al., 2007; Soo and Radke, 1986; Soo et al., 1984; Xu et al., 2017). Xu et al. (Xu et al., 2017) applied microfluidic to evaluate the effect of a nanofluid based on silica gel nanoparticles and a non-ionic surfactant (Tween 40) on emulsion stability and sweep efficiency in EOR processes. The combined effect of nanoparticles and surfactant prevented droplet coalescence and then, increased the emulsion stability in these systems. This effect was attributed to the synergy between the nanoparticles and surfactant in the oil-water interfaces and contributed to a higher areal sweep efficiency. Maurya et al. (Maurya et al., 2018) presented similar results related to the synergistic effect of surfactant and nanoparticles on oil-in-water (O/W) emulsion stabilization at reservoir conditions. The authors used silica gel nanoparticles, an anionic sodium dodecyl sulfate (SDS) and cationic cetyltrimethylammonium bromide (CTAB) as surfactants. The nanoparticles in the presence of the surfactant prevented the coalescence of the droplets and reduced the interfacial tension (IFT) at the oil-water interface

even at harsh reservoir conditions. Other authors indicated that the increase in oil recovery is due to the decreasing of IFT, the wettability alteration, the modification of flow pattern (Mohajeri et al., 2015) and the increase of viscosity of fluid injection (Cheraghian et al., 2017).

These applications were achieved through surfactant-nanoparticle systems using microfluidic devices without considering other variables that play a fundamental role in oil recovery applications such as the effect of injection rate and capillary number. Therefore, this work aims to investigate the main displacement mechanisms of the use of magnetic iron core-carbon shell nanoparticles and surfactant in enhanced oil recovery processes through microfluidic studies. For understanding the ratio between viscous and capillary forces in the presence of different injection fluids, the influence of three injection rates was evaluated: $0.1 \text{ ft}\cdot\text{day}^{-1}$ ($3.5\times 10^{-7} \text{ m}\cdot\text{s}^{-1}$), $1 \text{ ft}\cdot\text{day}^{-1}$ ($3.5\times 10^{-6} \text{ m}\cdot\text{s}^{-1}$), and $10 \text{ ft}\cdot\text{day}^{-1}$ ($3.5\times 10^{-5} \text{ m}\cdot\text{s}^{-1}$). Likewise, the interfacial tension crude oil/injection fluid and viscosity of the different injection fluids was measured for determining the capillary number. The formation and growth of fingers were monitored during the tests to evaluate the viscous fingering phenomenon. The injection fluids used for microfluidic tests were brine, surfactant mixture solution and nanofluid based on magnetic iron core-carbon shell nanoparticles and the surfactant mixture (Betancur et al., 2019a). All experiments were performed with a low nanoparticle concentration corresponding to $100 \text{ mg}\cdot\text{L}^{-1}$. It is expected that this study will allow for a better understanding of the displacement mechanisms during injection of a nanofluid and the role that play this type of smart fluids as an alternative chemical in EOR.

2. EXPERIMENTAL SECTION

2.1. Materials

2.1.1. Aqueous phase

A synthetic brine was employed for the preparation of the aqueous phase for all experiments and was formulated based on saltwater of a Colombian field. The total dissolved solids (TDS%) was 7850 mg·L⁻¹ and was selected based on the lowest interfacial tension value obtained in a previous study (Betancur et al., 2019b). Sodium chloride (NaCl 99%, PubChem, United States), potassium chloride (KCl ≥99%, PubChem, United States), dihydrate calcium chloride (CaCl₂·2H₂O ≥99%, Sigma-Aldrich, United States) and dihydrate magnesium chloride (MgCl₂·6H₂O ≥99%, Sigma-Aldrich, United States) were used for the preparation of the synthetic brine. Therefore, a synthetic brine with 6.46 g·L⁻¹ of NaCl, 0.136 g·L⁻¹ of KCl, 1.05 g·L⁻¹ of CaCl₂·2H₂O and 0.20 g·L⁻¹ of MgCl₂·2H₂O was used for all tests.

2.1.2. Crude oil

A Colombian intermediate crude oil with 33° API was used as the oleic phase. The crude oil has a dynamic viscosity of 117.6 cP and surface tension of 32.4 mN·m⁻¹ (3.24×10^{-2} N·m⁻¹) at 25 °C (298 K). The average content of saturated, aromatics, resins and asphaltenes (SARA) was determined with an Iatroscan MK-6 thin layer chromatograph based on IP 469 method (Institute, 2011). The content of saturated, aromatic, resins and asphaltenes were 53.9%, 26.2%, 12.2% and 7.7%, respectively (Betancur et al., 2019a).

2.1.3. Surfactant mixture

A mixture of a predominantly hydrophilic surfactant (S1) and a hydrophobic surfactant (S2) were employed for the surfactant mixture and were provided by Ecopetrol S.A. (Colombia) using

an 80:20 ratio based on previous works (Betancur et al., 2019a; Betancur et al., 2019b). For the preparation of surfactant mixture, S1 was added to the synthetic brine before adding the S2 surfactant. The hydrophilic-lipophilic balance (HLB) of the S1 and S2 surfactants mixture was determined through interfacial tension measurements with a force tensiometer, K11 (Krüss, Germany) according to the method proposed by Chun et al. (Chun and Martin, 1961). The HLB of the surfactant mixture was 18. Additional details about the preparation of surfactant mixture and its characterization can be found in the previous work of this research group (Betancur et al., 2019b).

2.1.4. Magnetic iron core-carbon shell nanoparticles

The magnetic iron core-carbon shell nanoparticles used for the nanoparticles-surfactant flooding were synthesized based on a one-step hydrothermal method (Betancur et al., 2019a; Moreno-Castilla et al., 2017). The mean particle size and surface area of the nanoparticles was 60 nm and $123 \text{ m}^2 \cdot \text{g}^{-1}$, respectively. The nanoparticles showed thermal stability at high temperature and high pressure according to the displacement tests carried out in a previous study (Betancur et al., 2019a). For the preparation of the nanoparticle-surfactant solution, the salts were dissolved in the deionized water followed by the surfactant mixture (surfactant S1 was added to the water and then, surfactant S2) and after, were dispersed the dry powder nanoparticles. Additional details about the synthesis and characterization of nanoparticles can be found in previous works (Betancur et al., 2019a; Betancur et al., 2019b). Table 1 summarizes the properties of the injection fluids used for the displacement tests at 25 °C (298 K).

Table 1. The viscosity of the injection fluid and interfacial tension values between the injection fluid and crude oil used for the displacement tests in a microfluidic device at 25 °C (298 K).

2.2. Methods

2.2.1. Design and fabrication of the microfluidic devices

To understand the effect of simultaneous use of the surfactant mixture and the magnetic iron core-carbon shell nanoparticles on oil recovery, several oil displacement tests were performed in microfluidic devices with a random network for different injection rates. The microfluidic porous media devices were fabricated in chemically inert polymer polydimethylsiloxane (PDMS). Details of the fabrication process have been described in previous work (Olmos et al., 2019). Briefly, in the first step, the microchannel network was designed using Layout Editor Software (Germany) and then, it was transferred to Thermal Imaging Layer (TIL). Subsequently, the female photopolymer mold (Fmold) fabrication was performed. Then, the photopolymer plate was washed and exposed to UVC light at 10 J for 17 min and UVA light at 4 J for 2 min on the front side. After, the epoxy resin mold was fabricated. For this, a mixture of epoxy resin and curing agent (Cristal-Tack, Novarchem – Argentina) was poured onto the female photopolymer mold to replicate the design in high relief. After curing, the epoxy resin mold (ERmold) was peeled off from the Fmold to form the male mold. Subsequently, a mixture of PDMS and curing agent in a 10:1 weight ratio (Sylgard 184 Silicone Elastomer Kit) was poured onto the ERmold and left in an oven at 40 °C (313 K) overnight. After curing, the PDMS replica was peeled off from the mold and holes for inlets and outlets of the channels were punched using a 1 mm diameter biopsy puncher (Integra Miltex®Ted Pella, Inc, United States). Finally, the PDMS replica was irreversibly bonded to a glass wafer after exposure to oxygen plasma produced by a BD-10A High-frequency generator (Electro-Technic Products, USA) for 120 s. The pattern and

the physical descriptions of the microfluidic devices used in the present study are presented in Figure 1 and Table 2, respectively. The design consists of an inlet and an outlet channel and a random network.

Figure 1. Design of the microfluidic device with the random network - magnified image of pores/grains in the porous media is shown in blue. The microfluidic porous media devices were fabricated in polydimethylsiloxane (PDMS) and glass.

Table 2. Measured dimensions and calculated areal properties for the microfluidic device with a random network.

2.2.2. Displacement tests

Displacements tests were carried out to evaluate the performance of a nanofluid based on a surfactant mixture and magnetic iron core-carbon shell nanoparticles for oil recovery. These tests consisted of the following stages: waterflooding (brine injection), surfactant flooding (surfactant mixture of S1 and S2) and nanoparticle-surfactant flooding (nanoparticles-surfactant solution) at the last stage. All tests were performed at 25 °C (298 K) temperature and atmospheric pressure. The injection rates of the brine, surfactant mixture, and nanoparticle-surfactant solution were $0.019 \mu\text{L}\cdot\text{min}^{-1}$ ($3.17\times 10^{-10} \text{ L}\cdot\text{s}^{-1}$), $0.19 \mu\text{L}\cdot\text{min}^{-1}$ ($3.17\times 10^{-9} \text{ L}\cdot\text{s}^{-1}$), and $1.9 \mu\text{L}\cdot\text{min}^{-1}$ ($3.17\times 10^{-8} \text{ L}\cdot\text{s}^{-1}$), corresponding to $0.1 \text{ ft}\cdot\text{day}^{-1}$, $1 \text{ ft}\cdot\text{day}^{-1}$, and $10 \text{ ft}\cdot\text{day}^{-1}$, respectively. These values were selected by choosing lower and higher values of the recommended injection rate of $1 \text{ ft}\cdot\text{day}^{-1}$ in a field application (De Ferrer, 2001). The synthetic brine, the surfactant mixture, and the magnetic

iron core-carbon shell nanoparticles were used for the preparation of the nanofluid and consisted in the addition of the salts to the deionized water, followed by the addition of surfactant mixture and then were added the dry powder nanoparticles (Betancur et al., 2019b). The samples were stirred at room temperature for 2 h. The concentration of the surfactant was determined based on the previous interfacial tension measurements (Betancur et al., 2019b), where the lowest crude oil/aqueous phase interfacial tension was obtained at a concentration of surfactant mixture of $2000 \text{ mg}\cdot\text{L}^{-1}$. The dosage of nanoparticles was $100 \text{ mg}\cdot\text{L}^{-1}$ (Betancur et al., 2019a). Before the displacement tests, the nanoparticle-surfactant solution was subjected to an ultrasonic bath (Elma Schmidbauer GmbH, Germany) for 1 h to disperse the nanoparticles in the solution.

Figure 2 shows a schematic representation of the microdevice visualization setup. For each oil displacement experiment, the microfluidic device was initially saturated with oil at an injection rate of $8.3 \text{ }\mu\text{L}\cdot\text{min}^{-1}$. Then, the oil was displaced by injecting the solution of study at a chosen injection rate using an OEM syringe pump (Chemyx Inc, United States), until steady-state conditions were obtained. A Canon T3-I Rebel digital camera was used to capture the images of the oil displacement tests. The images were created from a stack of multiple acquisitions over the area of the device (Avendaño et al., 2019; Rosero et al., 2018). Digital images were captured in 1-10 min intervals. Displacement experiments were performed in different microdevices for all fluids.

Figure 2. Schematic diagram of the microdevice visualization setup: (1) Digital camera, (2) microfluidic device, (3) light source, (4) OEM syringe pump, (5) waste storage, (6) computer. To

enable fluid flow through the microdevice, the microports were adjusted into the inlet and outlet chambers of the microfluidic devices.

2.2.3. Image Analysis

To calculate the oil recovery percentage of the flooding experiments, the standard image analysis using software Fiji -Image J (Schindelin et al., 2012) was used. Due to the high contrast between the oil and the injection fluids in the obtained images, it was possible to differentiate the two phases by defining a proper threshold range and convert them to binary images (Kargozarfard et al., 2019; Lacey et al., 2017; Rodríguez de Castro et al., 2015). Thus, the difference between the initial state of the black pixels and the final state was interpreted as recovered oil. Also, the breakthrough time (t_b) was calculated from the images. The t_b is defined as the earliest time at which the injecting fluid reaches the outlet of the chip in the microfluidic system (Kargozarfard et al., 2019).

2.2.4. Contact angle measurements

The contact angle tests were performed for evaluating the effect of the nanofluid based on the surfactant mixture and magnetic iron core-carbon shell nanoparticles on the wettability of both materials of microfluidic devices. PDMS and a glass slide were employed as the solid substrates. To evaluate the effect of the injection fluid on the wettability of both materials, PDMS and the glass wafer were submerged in each injection fluid for 24 h and then were dried at room temperature according to a modified procedure of previous works (Betancur et al., 2018; Giraldo et al., 2013). For contact angle tests, five drops of the crude oil were placed in different areas of

the solid substrate. The volume of the drop was controlled with a 5- μ L syringe. For determining the contact angle of the drop with the surface, sessile drop technique was used (Drelich, 2013). The contact angle tests were performed with an Attension theta optical tensiometer (Biolin Scientific, Sweden) at 25 °C (298 K) and atmospheric pressure. The images were processed using software Fiji -Image J. The same procedure was employed for establishing the wettability to the water of solid substrates (PDMS and glass) (Betancur et al., 2018).

3. RESULTS AND DISCUSSION

The microfluidic devices represent a micro-reservoir that is saturated with crude oil (He and Xu, 2016). Most of the reservoir rocks have a mixed state of wettability (Giraldo et al., 2013), i.e., there are not completely water-wet or oil-wet. Therefore, for representing more adequately a micro-reservoir, a hydrophobic (Ginn and Steinbock, 2003) (PDMS) and a hydrophilic surface (Kaneda et al., 2012) (glass wafer) were used for the fabrication of the microfluidic devices.

Incremental oil recovery is mainly attributed to the reduction of interfacial tension and wettability alteration (Agi et al., 2018; Maghzi et al., 2012; Morrow, 1990). In this sense, the effect of the injected fluids on the wettability alteration of PDMS and glass surfaces was evaluated by contact angle measurements using the sessile drop technique (Drelich, 2013). The injection fluids used for the contact angle experiments were brine, surfactant mixture of S1 and S2 and the nanoparticle-surfactant solution based on magnetic iron core-carbon shell nanoparticles and surfactant mixture of S1 and S2. As it can be seen in Figure 3, the PDMS and glass surfaces provide an oil-wet and mix-wet condition, respectively. After the treatments (i.e., brine, surfactant mixture, and nanoparticle-surfactant solution), the contact angles decreased for both surfaces, therefore the wettability is altered providing water-wet surfaces. On the PDMS,

the contact angle for brine decreases from 108.6 to 29.3° and 32.1° for surfactant mixture solution and nanoparticle-surfactant solution, respectively. Similarly, the contact angle for oil decreases from 41.6° to 22.5° (surfactant mixture solution) and 28.7° (nanoparticle-surfactant solution). Meanwhile, on the glass substrate, the contact angle of the drop of brine for both treatments decreases to values lower than 17°. These results indicate that the nanoparticle-surfactant solution is altering the wettability of the solid surfaces and are in agreement with work previously reported (Betancur et al., 2019a), where the mixture between the surfactant and magnetic iron core-carbon shell nanoparticles generates surfaces with a more water-wet condition. In addition, Maghzi et al. (Maghzi et al., 2012) reported an enhanced oil recovery by the effect of the water-wet surface due to glass surface coating with silica-nanoparticles.

The results suggest that the alteration of the wettability of PDMS and glass surfaces can be associated with the nature of the surfactants and these substrates. Therefore, the changes in the wettability of solid surfaces are determined by the orientation of the surfactant (Somasundaran and Zhang, 2006). According to the results of Figure 3, the glass surface showed a mixed state of wettability. Therefore, in the glass/air system, the charged head groups of surfactant molecules can be oriented towards the surface of the glass or the air. In this way, electrostatic or Van der Waals interactions (Parsegian, 2005) can exist between the charged head groups of the surfactant and the brine. Meanwhile, for the crude oil drop, the interactions with the glass surface coated with the surfactant can be Van der Waals type. Likewise, PDMS presented an oil-wet condition. The hydrophobic tail of the surfactant molecules is oriented towards PDMS surface with the charged head groups exposed. Therefore, the mechanisms responsible for the wettability alteration can be electrostatic interactions between the brine and the PDMS surface and Van der Waals between crude oil and PDMS surface.

The mechanisms associated with the alteration of wettability using nanoparticle-surfactant solution are similar to those described for surfactant systems. In this case, the systems consist in nanoparticles with adsorbed surfactant and free surfactant non-adsorbed onto the nanoparticles (Betancur et al., 2019a) and the wettability changes are determined by the orientation of these systems. Therefore, the substrates (i.e., glass or PDMS) can be coated with free surfactant or nanoparticles with adsorbed surfactant onto their surface. Magnetic iron core-carbon shell nanoparticles present hydrophobic groups in the surface, which favor the adsorption of surfactant molecules onto nanoparticles by the lipophilic group (Betancur et al., 2019b) and the hydrophilic groups can be exposed. Thus, the nanoparticles with adsorbed surfactant can present electrostatic interactions with the brine. Similarly, the interactions between the nanoparticles with adsorbed surfactant and the drop of crude oil can be of Van der Waals type. For the PDMS, Van der Waals interactions can exist between the nanoparticles with adsorbed surfactant and the drop of crude oil. The same type of interactions can occur between the nanoparticles with adsorbed surfactant and the glass surface. In this case, the interactions between the nanoparticles with adsorbed surfactant and the brine also are of electrostatic type.

Figure 3. Contact angle values for treated surfaces with surfactant mixture of S1 and S2 and nanoparticle –surfactant solution (based on the magnetic iron core-carbon shell nanoparticles and surfactant mixture of S1 and S2) and untreated surfaces: (a) Glass surface, (b) PDMS surface.

The sweep efficiency of different fluids under several injection rates was determined. The efficiency of each fluid in displacing oil is obtained by measuring the areal ratio of invaded

channels (white) to the area of the total channels, referred to as oil recovery. Figure 4 exhibits the oil displacement by waterflooding, surfactant flooding and nanoparticle-surfactant flooding, respectively, at the breakthrough time-varying the injection rate. The time required for the frontal saturation to reach the producing phase (i.e., breakthrough time) in porous media was obtained from the images. The experimental results obtained for the different stages of displacement tests at the breakthrough time and final recovery are shown in Table 2. As observed in Table 2, the oil recovery at the breakthrough time and injection rate of $0.19 \mu\text{L}\cdot\text{min}^{-1}$, was the highest compared with the injection rates of $0.019 \mu\text{L}\cdot\text{min}^{-1}$ and $1.9 \mu\text{L}\cdot\text{min}^{-1}$ for all displacement tests. These results are in agreement with the observations in Figure 4, where at the injection rate of $0.19 \mu\text{L}\cdot\text{min}^{-1}$ a more homogeneous sweep was observed. Higher oil recovery at breakthrough at $0.19 \mu\text{L}\cdot\text{min}^{-1}$ could be related to the residence time of the injection fluid in the porous media, facilitating a better interaction between fluid-fluid and fluid-surface. The breakthrough time for nanoparticle-surfactant flooding was 270 min, 102 min and 6 min at $0.019 \mu\text{L}\cdot\text{min}^{-1}$, $0.19 \mu\text{L}\cdot\text{min}^{-1}$, and $1.9 \mu\text{L}\cdot\text{min}^{-1}$, respectively. At the injection rate of $1.9 \mu\text{L}\cdot\text{min}^{-1}$, the residence time is the lowest among the injection rates, then the nanoparticle-surfactant solution does not have enough time to generate a significant effect on capillary forces. Likewise, the injection rate of $0.019 \mu\text{L}\cdot\text{min}^{-1}$ is a very low rate to achieve a considerable effect of the viscous forces and then, to increase the oil recovery.

The cumulative injection volume at the breakthrough time was 0.38 PVI, 0.55 PVI, and 0.73 PVI at the injection rate of $0.19 \mu\text{L}\cdot\text{min}^{-1}$ for waterflooding, surfactant flooding and nanoparticle-surfactant flooding, respectively. These results could be related to the fact that the displacement front is more stable at $0.19 \mu\text{L}\cdot\text{min}^{-1}$. In other words, the fingers caused by the difference of

viscosity of the displaced fluid and the injection fluid are wider and the sweep displacement is more efficient at breakthrough. On the other hand, the cumulative injection volume at the breakthrough was the highest for nanoparticle-surfactant flooding because of the synergy between the surfactant mixture and the nanoparticles. Both chemicals could be contributing to the viscous and capillary forces, which at the same time favor the oil recovery.

Figure 4. Distribution of fluids during waterflooding, surfactant-flooding (surfactant mixture of S1 and S2), and nanoparticle-surfactant flooding (nanofluid based on the magnetic iron core-carbon shell nanoparticles and surfactant mixture of S1 and S2) at the breakthrough time-varying the injection rate. The black area corresponds to the crude oil that is being displaced by the injection fluid (white).

Table 3. Experimental results obtained from waterflooding, surfactant-flooding (surfactant mixture of S1 and S2), and nanoparticle-surfactant flooding (nanofluid based on the magnetic iron core-carbon shell nanoparticles and surfactant mixture of S1 and S2) using microfluidic devices of PDMS and glass.

Figure 5 shows the oil distribution during the different stages of the displacement tests: waterflooding, surfactant flooding and nanoparticle-surfactant flooding at final state varying injection rate. At $0.019 \mu\text{L}\cdot\text{min}^{-1}$ injection rate, the injection fluid displaces the crude oil in a similar flow pattern. In addition, viscous fingering is observed in all cases at $0.019 \mu\text{L}\cdot\text{min}^{-1}$. The

viscous fingering is a phenomenon caused by viscosity and density differences between the fluids involved (Kueper and Frind, 1988), among other variables. In this study, the viscosity ratio between the displaced fluid (i.e., crude oil) and the displacing fluid (i.e., brine, surfactant mixture or nanoparticle-surfactant solution) is about 10. Thus, the injected fluid displaces a more viscous fluid (crude oil), the displacement front is unstable, resulting in viscous fingering (Peters and Flock, 1981).

Figures S1, S2, and S3 included in the supporting information show the microfluidic device images of oil distribution during water flooding, surfactant flooding, and nanoparticle-surfactant flooding at an injection rate of $0.019 \mu\text{L}\cdot\text{min}^{-1}$, $0.19 \mu\text{L}\cdot\text{min}^{-1}$, and $1.9 \mu\text{L}\cdot\text{min}^{-1}$, respectively. As shown in Figure S1, when 0.3 porous volume (PV) was injected at $0.019 \mu\text{L}\cdot\text{min}^{-1}$, the displacement front becomes unstable, resulting in viscous fingering. Similar behavior was also observed at $0.19 \mu\text{L}\cdot\text{min}^{-1}$ and $1.9 \mu\text{L}\cdot\text{min}^{-1}$ for waterflooding. However, as can be seen in Figure S2 and S3 of Supporting Information, at the injection rates of $0.19 \mu\text{L}\cdot\text{min}^{-1}$, and $1.9 \mu\text{L}\cdot\text{min}^{-1}$, respectively, there was a significant growth of the fingers after 0.3 PVI. This situation results in a more homogeneous flow pattern and consequently, there was an increase in the areal sweep efficiency.

On the other hand, as observed in Figure 5, at $0.19 \mu\text{L}\cdot\text{min}^{-1}$ and $1.9 \mu\text{L}\cdot\text{min}^{-1}$ injection rates the surfactant mixture and, nanoparticle-surfactant solution displace the crude oil in a more homogeneous flow pattern. In addition, the fingers start to grow for waterflooding and are almost nonexistent for surfactant flooding and nanoparticle-surfactant flooding. This growth of fingers increased the areal sweep efficiency and consequently, the oil recovery. As observed in Figure 5, the increase of injection rate implies a growth of the fingers. Kargozarfard et al. (Kargozarfard et

al., 2019), who studied three injection rates of $0.2 \text{ mL}\cdot\text{min}^{-1}$, $0.5 \text{ mL}\cdot\text{min}^{-1}$, and $1 \text{ mL}\cdot\text{min}^{-1}$ and its effect in areal sweep efficiency showed an equivalent trend with increasing injection rate.

Figure 5. Distribution of fluids during waterflooding, surfactant-flooding (surfactant mixture of S1 and S2), and nanoparticle-surfactant flooding (nanofluid based on the magnetic iron core-carbon shell nanoparticles and surfactant mixture of S1 and S2) at final state varying the injection rate. The black area corresponds to the crude oil that is being displaced by the injection fluid (white).

The pore-scale visualization of media during waterflooding, surfactant flooding and nanoparticle-surfactant flooding at an injection rate of $0.19 \mu\text{L}\cdot\text{min}^{-1}$ is depicted in Figure 6. The images of the waterflooding show that oil tends to adhere to the walls of pores and throats. In contrast, during the surfactant flooding and nanoparticle-surfactant flooding was observed that the thickness of the oil layer attached to walls decreased significantly. Indeed, the visualization of the microdevice during the nanoparticle-surfactant flooding indicates a higher sweep efficiency. Thus, the nanoparticle allows a higher release of oil from the walls of pores and throats, and therefore an increase in oil recovery was observed. It can be further concluded that during the waterflooding the system presents oil wettability, which implies a greater difficulty in mobilizing residual oil. The presence of surfactant generates a more water-wet condition that enhances oil recovery. The highest oil recovery from nanoparticle-surfactant fluid also can be associated with the ability of magnetic iron core-carbon shell nanoparticles to alter the wettability of porous media. These results are in agreement with the contact angle values observed in Figure 3. Another important factor that probably enhanced the sweep efficiency is

related to the formation of the emulsions. The contact of the surfactant with the oil and the shearing forces can cause emulsify the oil to O/W emulsions or bi-continuous micro emulsion, which enhance the oil deformability and decrease the flow resistance giving as result an enhanced oil recovery (Ahmed and Elraies, 2018).

Figure 6. Detailed view of the pore space occupation after waterflooding, surfactant flooding (surfactant mixture of S1 and S2) and nanoparticles-surfactant flooding (nanofluid based on the magnetic iron core-carbon shell nanoparticles and surfactant mixture of S1 and S2) at breakthrough time. The black area corresponds to the crude oil that is being displaced by the injection fluid (white). Flow injection: $0.19 \mu\text{L}\cdot\text{min}^{-1}$.

Figure 7 shows the oil recovery curves for waterflooding, surfactant flooding and nanoparticle-surfactant flooding at different injection rates: $0.019 \mu\text{L}\cdot\text{min}^{-1}$, $0.19 \mu\text{L}\cdot\text{min}^{-1}$, and $1.9 \mu\text{L}\cdot\text{min}^{-1}$. As observed, the oil recovery decreased in the order: $1.9 \mu\text{L}\cdot\text{min}^{-1} > 0.19 \mu\text{L}\cdot\text{min}^{-1} > 0.019 \mu\text{L}\cdot\text{min}^{-1}$. The increase of the injection rate of the injection fluid favors the viscous forces, which produces an increase of capillary number. The experimental results also showed that the oil recovery decreased in the order: nanoparticle-surfactant flooding $>$ surfactant flooding $>$ waterflooding in all different flow rate cases. Figure 7a presents the oil recovery at an injection rate of $0.019 \mu\text{L}\cdot\text{min}^{-1}$. At this injection rate, the oil recovery percentages were 34, 36 and 41% for waterflooding, surfactant flooding and nanoparticle-surfactant flooding, respectively. This similar behavior can be associated with a low injection rate. At this injection rate, the capillary number does not change significantly for increasing the oil recovery percentage. These results are in a good agreement with the low areal sweep efficiency caused by viscous fingering

phenomenon at $0.019 \mu\text{L}\cdot\text{min}^{-1}$. The behavior reported in the literature, the oil recovery by waterflooding is known to be low for the adverse viscosity ratio between the oil and the injected water, especially in heavy crude oils (Mai and Kantzas, 2009).

Meanwhile, at injection rates of $0.19 \mu\text{L}\cdot\text{min}^{-1}$ (Figure 7b), and $1.9 \mu\text{L}\cdot\text{min}^{-1}$ (Figure 7c), waterflooding showed significant differences in the percentages of oil recovery than those obtained with surfactant flooding and nanoparticle-surfactant flooding. In addition, it is observed that nanoparticle-surfactant flooding achieved the highest oil recovery percentages among the evaluated treatments. The highest oil recovery percentage was obtained for the nanoparticle-surfactant flooding system at an injection rate of $1.9 \mu\text{L}\cdot\text{min}^{-1}$. This increase in oil recovery can be related to the synergy between the nanoparticles and the surfactant mixture and the changes of the capillary number using nanoparticles in the injection fluid. On the other hand, the oil recovery percentage can be associated with the residence time of each injection fluid in the porous medium. In Figure 7, it is observed that at the injection rate of $1.9 \mu\text{L}\cdot\text{min}^{-1}$ (Figure 7c), the oil recovery is maximum after of 15 PVI. This behavior can occur due to surfactant mixture or nanoparticle-surfactant solution do not have enough time for generating a significantly effect on interfacial tension or wettability of porous medium. In contrast, as observed in Figure 7a, at the injection rate of $0.019 \mu\text{L}\cdot\text{min}^{-1}$, the percentage of oil recovery is maximum after approximately 1 PVI. At $0.019 \mu\text{L}\cdot\text{min}^{-1}$, the injected fluid (surfactant mixture or nanoparticle-surfactant solution) can interact for longer with the porous medium and the crude oil, which favor the increase of oil recovery at lower PVI.

Figure 7. Oil recovery curves as a function of pore volumes injected for the waterflooding, surfactant flooding (surfactant mixture of S1 and S2) and the nanoparticle–surfactant flooding (nanofluid based on the magnetic iron core-carbon shell nanoparticles and surfactant mixture of

S1 and S2) at different injection rates: (a) $0.019 \mu\text{L}\cdot\text{min}^{-1}$, (b) $0.19 \mu\text{L}\cdot\text{min}^{-1}$, and (c) $1.9 \mu\text{L}\cdot\text{min}^{-1}$

¹. The displacement tests were conducted in a microfluidic device of PDMS and glass.

Oil recovery as a function of capillary number for brine, surfactant mixture and nanoparticle-surfactant injection fluid at different injection rates is shown in Figure 8. As observed, the capillary number decreases in the following order: $1.9 \mu\text{L}\cdot\text{min}^{-1} > 0.19 \mu\text{L}\cdot\text{min}^{-1} > 0.019 \mu\text{L}\cdot\text{min}^{-1}$. These results are in agreement with the oil recovery percentages presented in Figure 7, where the highest capillary number was obtained for the injection rate of $1.9 \mu\text{L}\cdot\text{min}^{-1}$. Similarly, the capillary number varied from 6.3×10^{-8} to 6.3×10^{-6} for brine, 1.4×10^{-6} to 1.4×10^{-4} for surfactant mixture and, 1.4×10^{-4} to 1.4×10^{-2} for nanoparticle-surfactant fluid injection. The field data indicates that the oil recovery percentage is very low when the capillary number is below 10^{-6} and is near to 100% when the capillary number is above 10^{-3} (Salager, 2005). Although all experiments do not produce exactly the same transition, increasing the capillary number by three or four orders of magnitude can increase oil recovery by about 100% (Salager, 2005). Indeed, the capillary number for nanoparticle-surfactant flooding at $1.9 \mu\text{L}\cdot\text{min}^{-1}$ was 1.4×10^{-2} and was obtained an oil recovery percentage of 84%. Meanwhile, at an injection rate of $1.9 \mu\text{L}\cdot\text{min}^{-1}$, capillary number and oil recovery obtained with waterflooding were 6.3×10^{-6} and 54%, respectively. These capillary numbers are in agreement with the typical values of the capillary number for reservoir conditions (Satter and Iqbal, 2015). As observed in Table 1, the nanoparticle-surfactant solution presented a viscosity slightly higher than that observed with the brine and surfactant mixture. Likewise, the nanoparticle-surfactant solution showed the lowest interfacial tension crude oil/aqueous phase at $25 \text{ }^\circ\text{C}$ (298 K) among the treatments. These results are in agreement with those obtained by several authors, who indicated that in practice high

values of capillary number necessarily imply with low interfacial tension of crude oil/water system (Melrose, 1974; Taber, 1969). Additionally, the high injection rate increases the capillary number, which facilitates oil recovery.

Figure 8. Oil recovery as a function of capillary number for waterflooding, surfactant flooding (surfactant mixture of S1 and S2) and nanoparticles-surfactant flooding (nanofluid based on the magnetic iron core-carbon shell nanoparticles and surfactant mixture of S1 and S2) at injection rates of $0.019 \mu\text{L}\cdot\text{min}^{-1}$, $0.19 \mu\text{L}\cdot\text{min}^{-1}$, and $1.9 \mu\text{L}\cdot\text{min}^{-1}$.

4. CONCLUSIONS

Oil displacements tests were performed in a microfluidic device in order to evaluate the effect of magnetic iron core-carbon shell nanoparticles and a surfactant mixture for being applied as an EOR method. The different stages of the displacement tests were waterflooding, emulating a secondary recovery process, and surfactant and nanoparticle-surfactant flooding, which were applied to emulate EOR methods. The influence of the injection rate was evaluated and was varied at different rates of $0.019 \mu\text{L}\cdot\text{min}^{-1}$, $0.19 \mu\text{L}\cdot\text{min}^{-1}$ and $1.9 \mu\text{L}\cdot\text{min}^{-1}$. Mechanisms as the wettability alteration of porous media, decreasing of interfacial tension, increasing of viscosity and the modification of flow patterns led a successful oil recovery enhancing. Recovery by waterflooding was the lowest among the evaluated systems. This behavior can be related to the viscous fingering observed due to the viscosity differences between the displaced and the injection fluid. The final oil recovery was the highest for the injection rate of $1.9 \mu\text{L}\cdot\text{min}^{-1}$ among 0.019 and $0.19 \mu\text{L}\cdot\text{min}^{-1}$. The increase of the injection rate favored the viscous force of the

injection fluid and then, there was an increase in the capillary number. Indeed, the capillary number for nanoparticle-surfactant flooding at $1.9 \mu\text{L}\cdot\text{min}^{-1}$ was 1.4×10^{-2} and was obtained an oil recovery percentage of 84%. The increase of capillary number could be associated with the synergy between the surfactant mixture and nanoparticles for reducing the interfacial tension crude oil/aqueous phase. In addition, in all cases, nanoparticle-surfactant flooding led the highest oil recovery among the evaluated injection fluids. At the injection rate of $0.019 \mu\text{L}\cdot\text{min}^{-1}$ did not present significant changes in the capillary number due to the low injection rate and viscous fingering phenomenon was observed.

The distribution of fluids during waterflooding, surfactant flooding and nanoparticle-surfactant flooding showed significant differences after 0.3 PVI of the injection fluid. At an injection fluid of $0.019 \mu\text{L}\cdot\text{min}^{-1}$, the viscous fingering was notable for all cases and was significantly reduced at $0.19 \mu\text{L}\cdot\text{min}^{-1}$ and $1.9 \mu\text{L}\cdot\text{min}^{-1}$. Similar results were observed at the breakthrough time. However, the distribution of fluids images showed growth of fingers for surfactant flooding and nanoparticle-surfactant flooding even after 0.3 PVI. In these cases, the displacement front was more stable and then, a significant increase in oil recovery was observed.

A decrease in IFT of crude oil/brine system from $23.4 \text{ mN}\cdot\text{m}^{-1}$ to $2.7 \text{ mN}\cdot\text{m}^{-1}$ and $0.03 \text{ mN}\cdot\text{m}^{-1}$ for the crude oil-surfactant and crude oil-nanoparticle-surfactant, respectively was observed. The addition of surfactant and a mixture of nanoparticles and surfactant slightly increased the brine viscosity. That is a surfactant and a mixture of nanoparticles and surfactant increase 60% and 64 % of the brine viscosity, respectively. Therefore, oil mobility control was influenced by the viscosity, which resulted in a better mobility ratio and less viscosity difference between oil and injection fluid. On the other hand, the nanoparticle-surfactant solution achieved to modify the wettability of the substrates of microfluidic device. These results were achieved at a nanoparticle

concentration of $100 \text{ mg}\cdot\text{L}^{-1}$, which indicates that the simultaneous use of nanoparticles and surfactants could become a cost-effective alternative in EOR processes.

5. ACKNOWLEDGMENTS

Ph.D. (c) Stefania Betancur wants to acknowledge to the Departamento Administrativo de Ciencia, Tecnología e Innovación de Colombia (COLCIENCIAS) for the scholarship received from call 727-2015. The authors thank the financial support from CONICET (PIP2015) and ANPCyT (PICT 4819 and 1021). The authors also acknowledge Universidad Nacional de Colombia, Universidad de Granada, agreement 3010388 of 2017 with Ecopetrol S.A., agreement 647 of 2015 and 064 of 2018 with COLCIENCIAS and Agencia Nacional de Hidrocarburos (ANH), Ministerio de Ciencia, Innovación y Universidades (Spain), FEDER, contract number RTI2018-099224-B-I00 and Junta de Andalucía Ref. RMN-172 for the support provided.

6. REFERENCES

- Afolabi, F., 2015. Cost-Effective Chemical Enhanced Oil Recovery. *International Journal of Petroleum and Petrochemical Engineering (IJPPE)*, 1(2): 1-11.
- Agi, A., Junin, R. and Gbadamosi, A., 2018. Mechanism governing nanoparticle flow behaviour in porous media: insight for enhanced oil recovery applications. *International Nano Letters*, 8(2): 49-77.
- Ahmed, S. and Elraies, K.A., 2018. Microemulsion in Enhanced Oil Recovery. *Science and Technology Behind Nanoemulsions*: 145.
- Alvarado, V. and Manrique, E., 2010. Enhanced oil recovery: an update review. *Energies*, 3(9): 1529-1575.

- Avendaño, J., Lima, N., Quevedo, A. and Carvalho, M., 2019. Effect of Surface Wettability on Immiscible Displacement in a Microfluidic Porous Media. *Energies*, 12(4): 664.
- Baret, J.-C., Kleinschmidt, F., El Harrak, A. and Griffiths, A.D.J.L., 2009. Kinetic aspects of emulsion stabilization by surfactants: a microfluidic analysis. 25(11): 6088-6093.
- Bennetzen, M.V. and Mogensen, K., 2014. Novel applications of nanoparticles for future enhanced oil recovery, International petroleum technology conference. International Petroleum Technology Conference.
- Betancur, S. et al., 2019a. Effect of Magnetic Iron Core–Carbon Shell Nanoparticles in Chemical Enhanced Oil Recovery for Ultralow Interfacial Tension Region. 33(5): 4158-4168.
- Betancur, S., Franco, C.A. and Cortés, F.B., 2018. Wettability alteration in sandstone cores using nanofluids based on silica gel. Formation damage in oil and gas reservoirs: Nanotechnology applications for its inhibition/remediation. Nova Science Publishers, New York, 151-182 pp.
- Betancur, S. et al., 2019b. Importance of the Nanofluid Preparation for Ultra-Low Interfacial Tension in Enhanced Oil Recovery Based on Surfactant–Nanoparticle–Brine System Interaction.
- Cheraghian, G., Kiani, S., Nassar, N.N., Alexander, S. and Barron, A.R., 2017. Silica nanoparticle enhancement in the efficiency of surfactant flooding of heavy oil in a glass micromodel. *Industrial & Engineering Chemistry Research*, 56(30): 8528-8534.
- Christian, P., Von der Kammer, F., Baalousha, M. and Hofmann, T., 2008. Nanoparticles: structure, properties, preparation and behaviour in environmental media. *Ecotoxicology*, 17(5): 326-343.

- Chun, A.H. and Martin, A.N., 1961. Measurement of hydrophile-lipophile balance of surface-active agents. *Journal of pharmaceutical sciences*, 50(9): 732-736.
- De Ferrer, M.P., 2001. Inyección de agua y gas en yacimientos petrolíferos. Ediciones astro data SA Maracaibo, Venezuela.
- Drelich, J., 2013. Guidelines to measurements of reproducible contact angles using a sessile-drop technique. *Surface innovations*, 1(4): 248-254.
- Ehtesabi, H., Ahadian, M.M., Taghikhani, V. and Ghazanfari, M.H., 2013. Enhanced heavy oil recovery in sandstone cores using TiO₂ nanofluids. *Energy & Fuels*, 28(1): 423-430.
- Ginn, B.T. and Steinbock, O., 2003. Polymer surface modification using microwave-oven-generated plasma. *Langmuir*, 19(19): 8117-8118.
- Giraldo, J., Benjumea, P., Lopera, S., Cortés, F.B. and Ruiz, M.A., 2013. Wettability alteration of sandstone cores by alumina-based nanofluids. *Energy & Fuels*, 27(7): 3659-3665.
- Gogoi, S. and Gogoi, S.B., 2019. Review on microfluidic studies for EOR application. *Journal of Petroleum Exploration and Production Technology*: 1-15.
- He, K. and Xu, L., 2016. Determining treatment fluid composition using a mini-reservoir device. Google Patents.
- Institute, E., 2011. IP 469: Determination of Saturated, Aromatic and Polar Compounds in Petroleum Products by Thin Layer Chromatography and Flame Ionization Detection.
- Jang, S.B. and Chon, B.H., 2014. Surfactant-polymer flooding characteristics for heavy oil recovery with varying injection volumes of surfactant and polymer. *Geosystem Engineering*, 17(2): 150-156.
- Kaneda, S. et al., 2012. Modification of the glass surface property in PDMS-glass hybrid microfluidic devices. *Analytical Sciences*, 28(1): 39-39.

- Kargozarfard, Z., Riazi, M. and Ayatollahi, S., 2019. Viscous fingering and its effect on areal sweep efficiency during waterflooding: an experimental study. *Petroleum Science*, 16(1): 105-116.
- Kazemzadeh, Y., Shojaei, S., Riazi, M. and Sharifi, M., 2019. Review on application of nanoparticles for EOR purposes: A critical review of the opportunities and challenges. *Chinese Journal of Chemical Engineering*, 27(2): 237-246.
- Kenzhekhanov, S., 2016. Chemical EOR process visualization using NOA81 micromodels, Colorado School of Mines. Arthur Lakes Library.
- Kueper, B.H. and Frind, E.O., 1988. An overview of immiscible fingering in porous media. *Journal of contaminant Hydrology*, 2(2): 95-110.
- Lacey, M., Hollis, C., Oostrom, M. and Shokri, N., 2017. Effects of pore and grain size on water and polymer flooding in micromodels. *Energy & Fuels*, 31(9): 9026-9034.
- Li, S., Genys, M., Wang, K. and Torsæter, O., 2015. Experimental study of wettability alteration during nanofluid enhanced oil recovery process and its effect on oil recovery, SPE Reservoir Characterisation and Simulation Conference and Exhibition. Society of Petroleum Engineers.
- Maghzi, A., Mohammadi, S., Ghazanfari, M.H., Kharrat, R. and Masihi, M., 2012. Monitoring wettability alteration by silica nanoparticles during water flooding to heavy oils in five-spot systems: A pore-level investigation. *Experimental Thermal and Fluid Science*, 40: 168-176.
- Mai, A. and Kantzas, A., 2009. Heavy oil waterflooding: effects of flow rate and oil viscosity. *Journal of Canadian Petroleum Technology*, 48(03): 42-51.

- Maurya, N.K., Mandal, A.J.C.E.R. and Design, 2018. Investigation of synergistic effect of nanoparticle and surfactant in macro emulsion based EOR application in oil reservoirs. 132: 370-384.
- Melrose, J., 1974. Role of capillary forces in detennining microscopic displacement efficiency for oil recovery by waterflooding. *Journal of Canadian Petroleum Technology*, 13(04).
- Meybodi, H.E., Kharrat, R. and Wang, X.J.T.i.p.m., 2011. Study of microscopic and macroscopic displacement behaviors of polymer solution in water-wet and oil-wet media. 89(1): 97-120.
- Moghadam, T.F., Azizian, S. and Wettig, S., 2015. Synergistic behaviour of ZnO nanoparticles and gemini surfactants on the dynamic and equilibrium oil/water interfacial tension. *Physical Chemistry Chemical Physics*, 17(11): 7122-7129.
- Mohajeri, M., Hemmati, M., Shekarabi, A.S.J.J.o.p.S. and engineering, 2015. An experimental study on using a nanosurfactant in an EOR process of heavy oil in a fractured micromodel. 126: 162-173.
- Moreno-Castilla, C., García-Rosero, H., Carrasco-Marín, F.J.C., Physicochemical, S.A. and Aspects, E., 2017. Synthesis and characterization of solid polymer and carbon spheres derived from an emulsion polymerization reaction of different phenolic compounds with formaldehyde. 520: 488-496.
- Morrow, N.R., 1990. Wettability and its effect on oil recovery. *Journal of petroleum technology*, 42(12): 1,476-1,484.
- Moslemizadeh, A. et al., 2016. Novel bio-based surfactant for chemical enhanced oil recovery in montmorillonite rich reservoirs: Adsorption behavior, interaction impact, and oil recovery studies. *Chemical Engineering Research and Design*, 109: 18-31.

- Muggeridge, A. et al., 2014. Recovery rates, enhanced oil recovery and technological limits. *Philosophical Transactions of the Royal Society A: Mathematical, Physical and Engineering Sciences*, 372(2006): 20120320.
- Olmos, C.M. et al., 2019. Epoxy resin mold and PDMS microfluidic devices through photopolymer flexographic printing plate. *Sensors and Actuators B: Chemical*, 288: 742-748.
- Parsegian, V.A., 2005. Van der Waals forces: a handbook for biologists, chemists, engineers, and physicists. Cambridge University Press.
- Peters, E.J. and Flock, D.L., 1981. The onset of instability during two-phase immiscible displacement in porous media. *Society of Petroleum Engineers Journal*, 21(02): 249-258.
- Priest, C., Reid, M.D., Whitby, C.P.J.J.o.c. and science, i., 2011. Formation and stability of nanoparticle-stabilised oil-in-water emulsions in a microfluidic chip. 363(1): 301-306.
- Rodríguez de Castro, A., Shokri, N., Karadimitriou, N., Oostrom, M. and Joekar-Niasar, V., 2015. Experimental study on nonmonotonicity of Capillary Desaturation Curves in a 2-D pore network. *Water Resources Research*, 51(10): 8517-8528.
- Romero-Zeron, L.B., Kantzas, A.J.S.R.E. and Engineering, 2007. The effect of wettability and pore geometry on foamed-gel-blockage performance. 10(02): 150-163.
- Rosero, G. et al., 2018. Design and analysis of different models of microfluidic devices evaluated in Enhanced Oil Recovery (EOR) assays. *Matéria (Rio de Janeiro)*, 23(2).
- Salager, J.-L., 2005. Recuperación mejorada del petróleo. ULA.[S357-C].
- Satter, A. and Iqbal, G.M., 2015. Reservoir Engineering: The fundamentals, simulation, and management of conventional and unconventional recoveries. Gulf Professional Publishing.

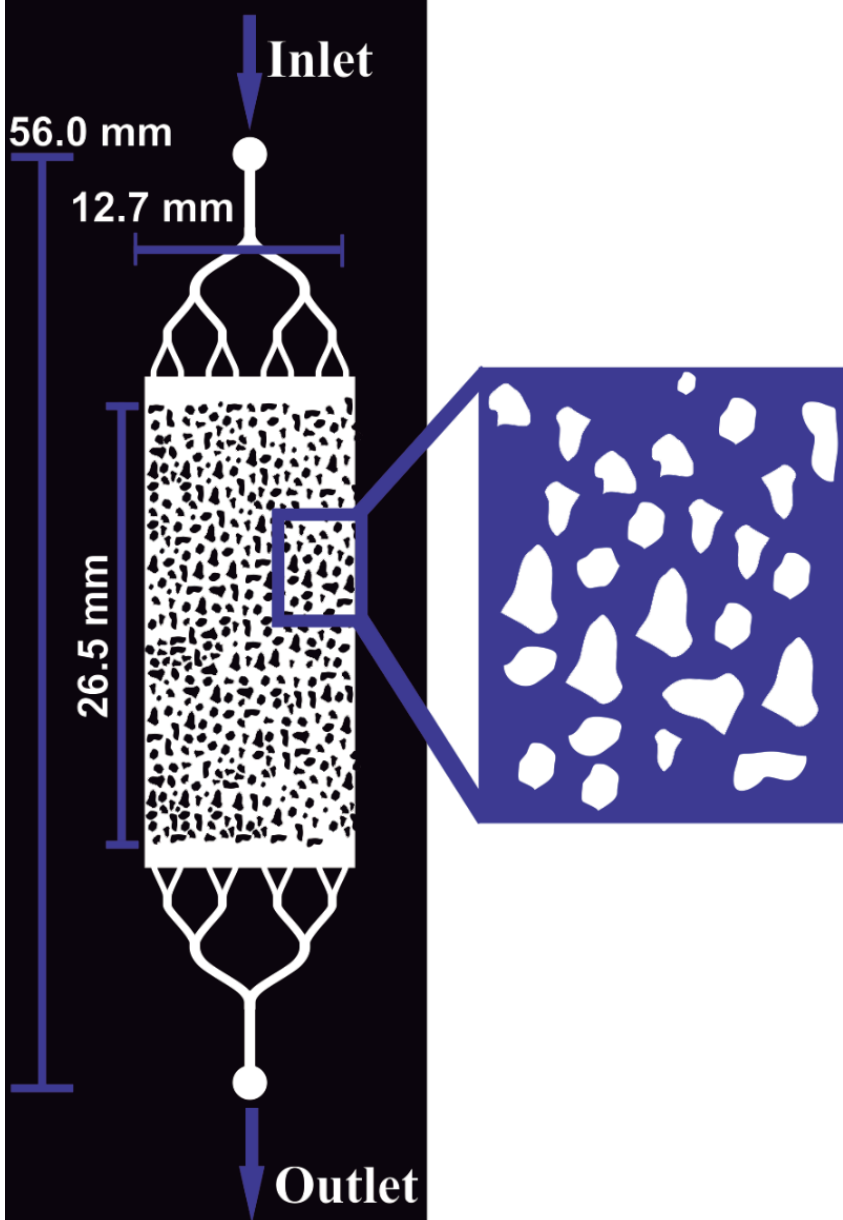
- Schindelin, J. et al., 2012. Fiji: an open-source platform for biological-image analysis. *Nature methods*, 9(7): 676.
- Sheng, J., 2010. *Modern chemical enhanced oil recovery: theory and practice*. Gulf Professional Publishing.
- Somasundaran, P. and Zhang, L., 2006. Adsorption of surfactants on minerals for wettability control in improved oil recovery processes. *Journal of Petroleum Science and Engineering*, 52(1-4): 198-212.
- Soo, H. and Radke, C.J.C.E.S., 1986. A filtration model for the flow of dilute, stable emulsions in porous media—I. Theory. 41(2): 263-272.
- Soo, H., Radke, C.J.J.I. and fundamentals, e.c., 1984. Flow mechanism of dilute, stable emulsions in porous media. 23(3): 342-347.
- Taber, J., 1969. Dynamic and static forces required to remove a discontinuous oil phase from porous media containing both oil and water. *Society of Petroleum Engineers Journal*, 9(01): 3-12.
- Xu, K., Zhu, P., Colon, T., Huh, C. and Balhoff, M.J.S.J., 2017. A microfluidic investigation of the synergistic effect of nanoparticles and surfactants in macro-emulsion-based enhanced oil recovery. 22(02): 459-469.
- Zargartalebi, M., Barati, N. and Kharrat, R., 2014. Influences of hydrophilic and hydrophobic silica nanoparticles on anionic surfactant properties: Interfacial and adsorption behaviors. *Journal of Petroleum Science and Engineering*, 119: 36-43.
- Zargartalebi, M., Kharrat, R. and Barati, N., 2015. Enhancement of surfactant flooding performance by the use of silica nanoparticles. *Fuel*, 143: 21-27.

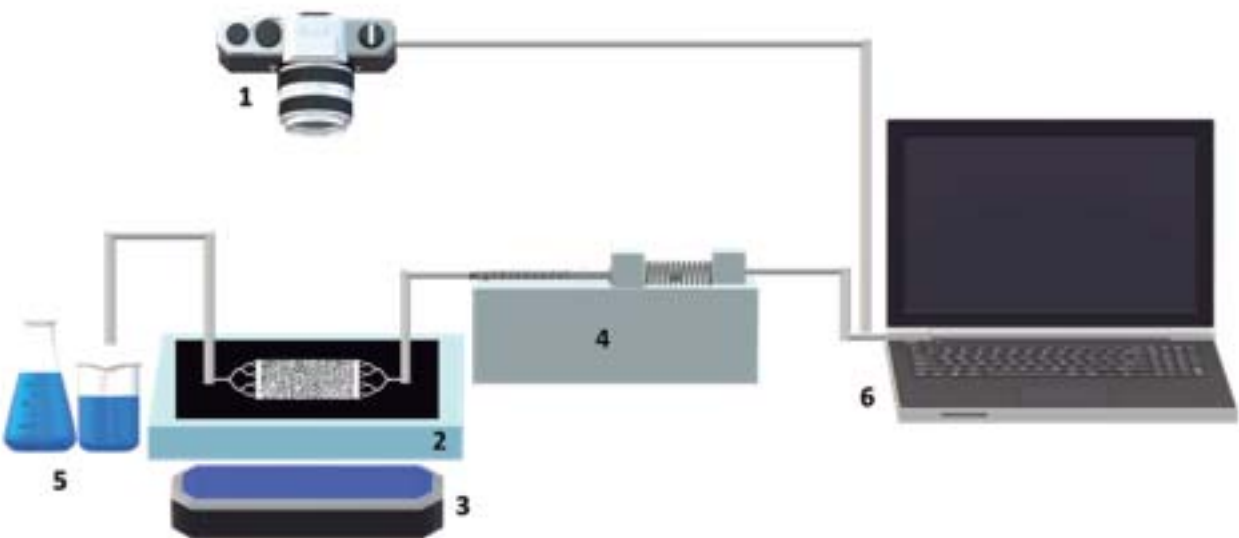
Injection Fluid	Viscosity (cP)	Interfacial tension(mN·m⁻¹)
Brine	4.34	23.40
Surfactant mixture	10.72	2.70
Nanoparticle-surfactant solution	12.00	0.03

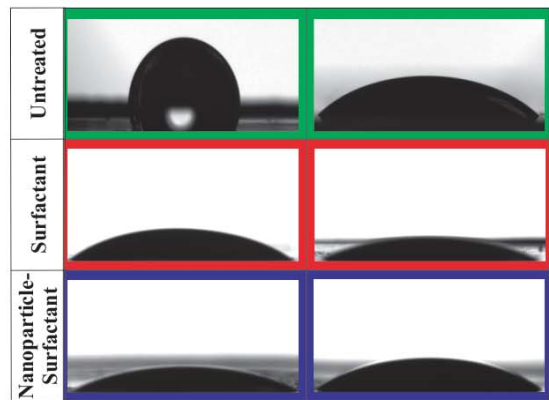
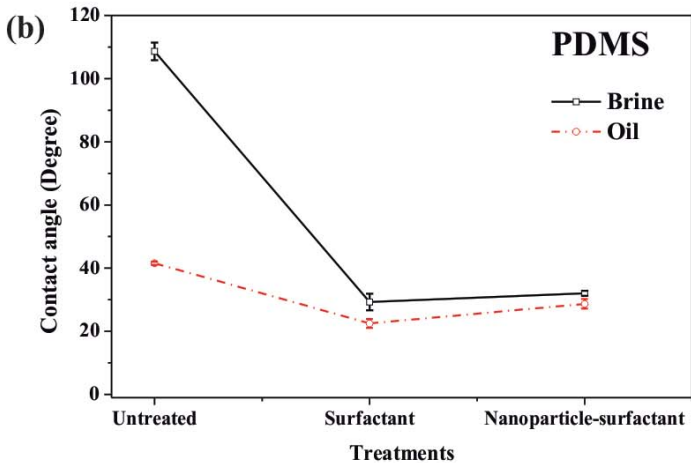
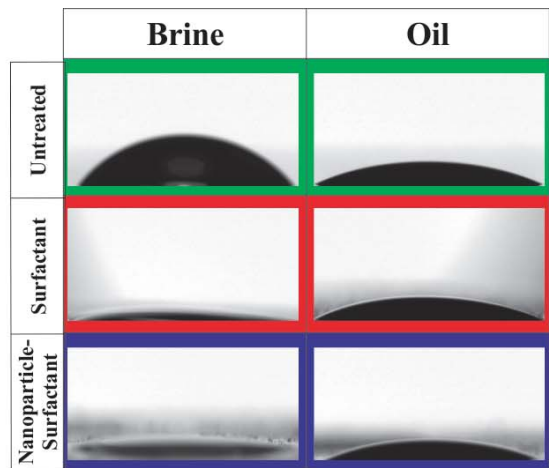
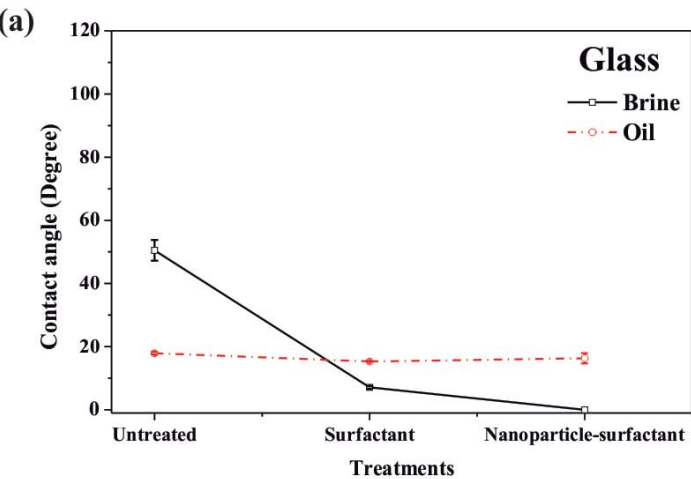
Journal Pre-proof

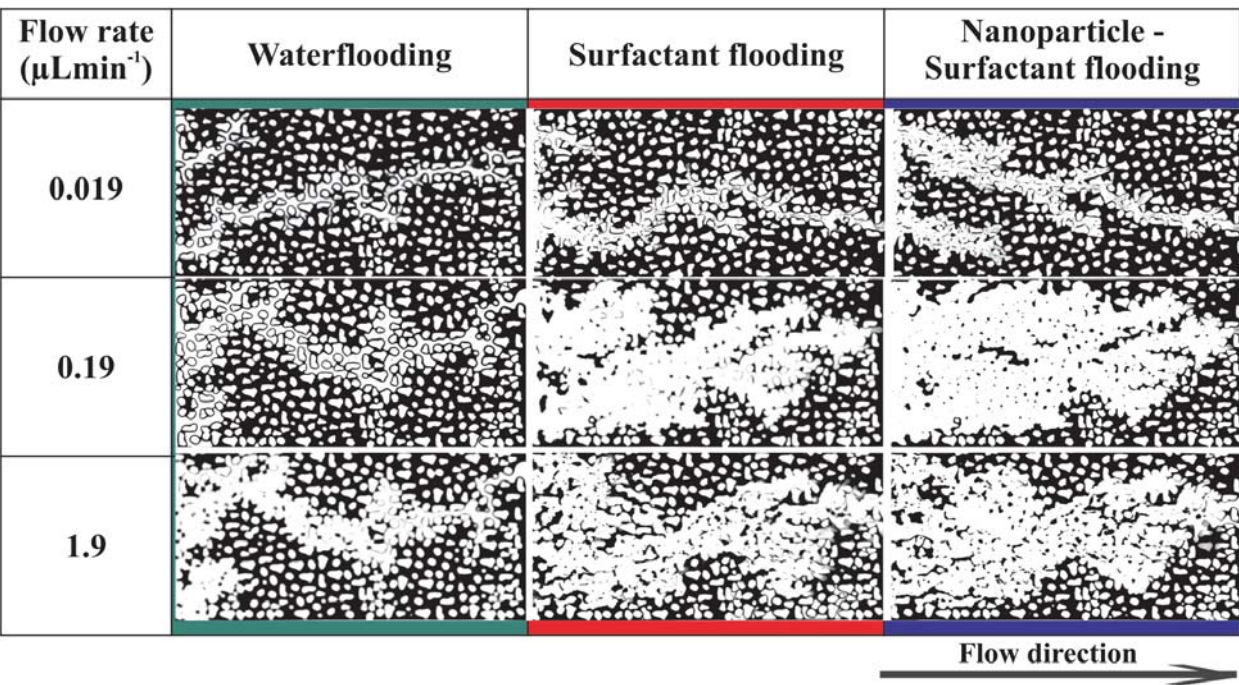
Description	Dimensions
Device length (mm)	56.0
Porous medium length (mm)	26.5
Width (mm)	12.7
Average depth (μm)	99.9
Pore volume (μL)	23.9
Porosity (%)	70.9
Absolute permeability (D)	5.71
Pore throat size (mm)	0.1 – 0.6
Grain size range (mm)	0.2 – 1.2


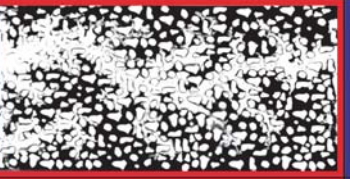




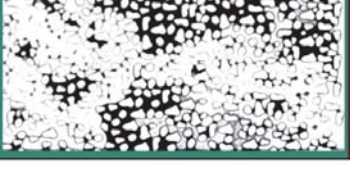


Injection	Injection rate ($\mu\text{L}\cdot\text{min}^{-1}$)	Breakthrough Time (min)	Cumulative injection volume at breakthrough time (PVI)	Oil recovery at breakthrough time (%)	Final oil recovery (%)
Waterflooding	0.019	304	0.24	17.4	34.1
	0.19	47	0.38	26.0	38.7
	1.90	5	0.40	29.8	54.1
Surfactant flooding	0.019	251	0.20	18.0	35.9
	0.19	69	0.55	51.8	62.9
	1.90	6	0.48	43.6	79.4
Nanoparticle – Surfactant flooding	0.019	270	0.22	22.0	40.5
	0.19	102	0.81	56.9	73.9
	1.90	6	0.48	46.7	84.0




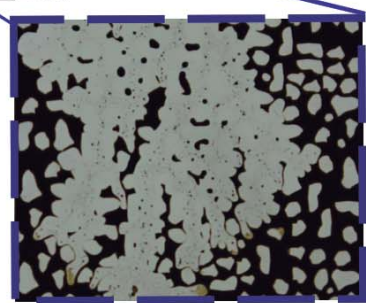
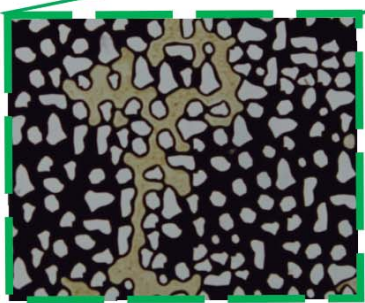
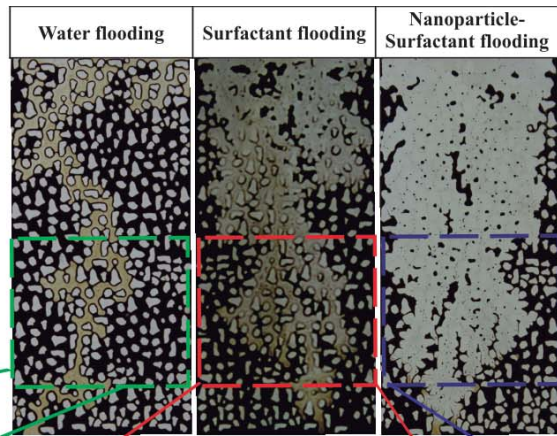


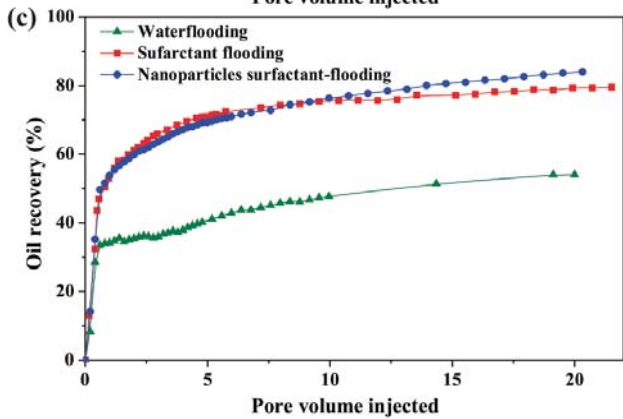
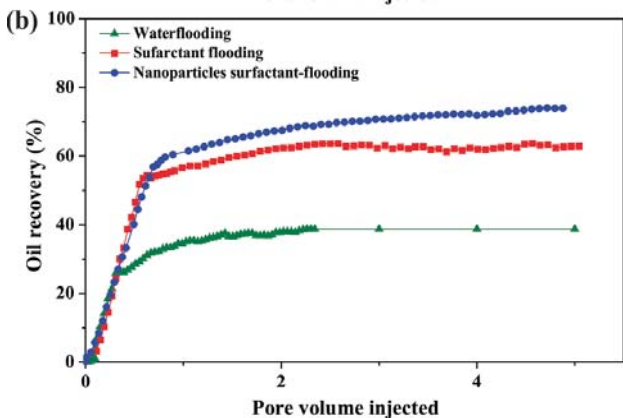
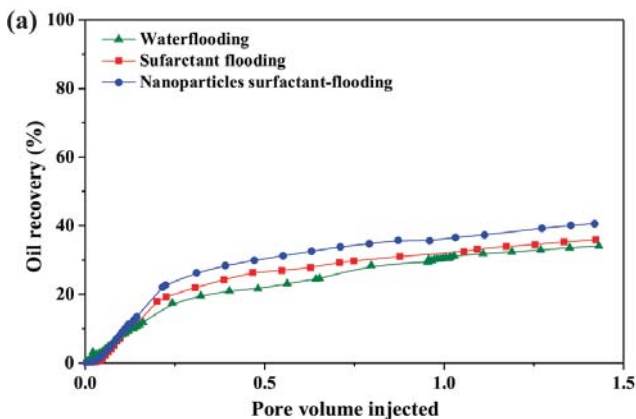


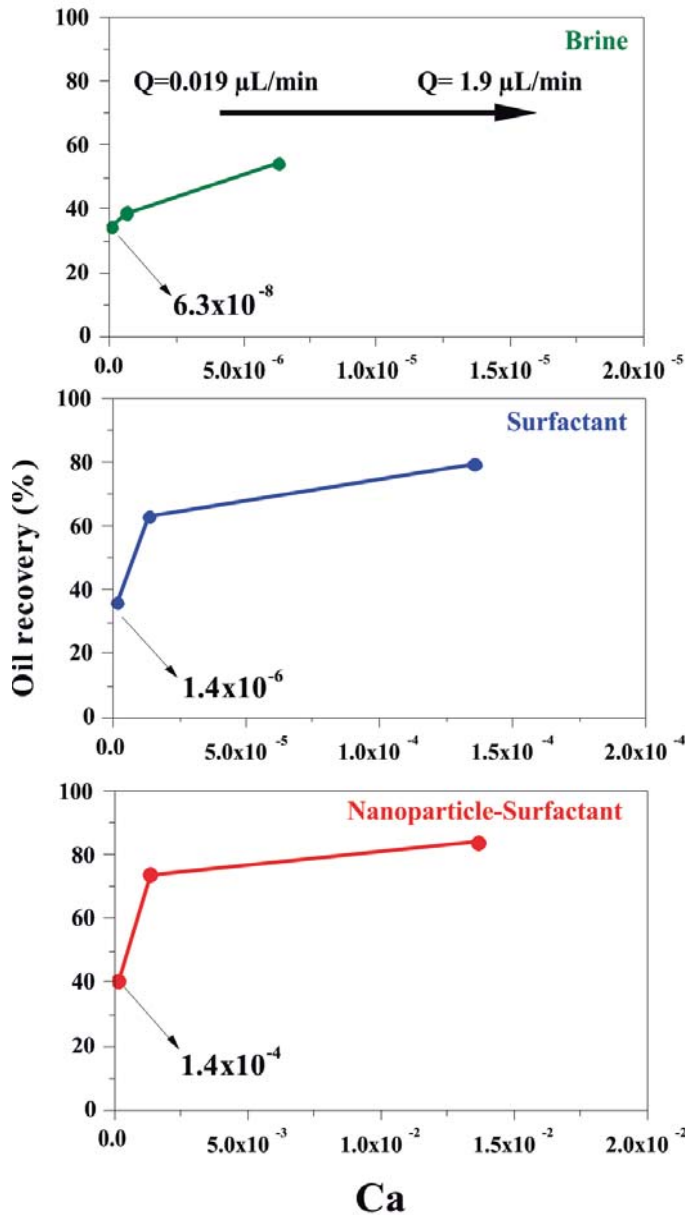


Flow rate (μLmin^{-1})	Waterflooding	Surfactant flooding	Nanoparticle - Surfactant flooding
0.019			
0.19			
1.9			

Flow direction 







HIGHLIGHTS

- A microfluidic investigation using nanoparticles and surfactant was performed for oil recovery.
- The increase in the injection rate increased capillary number and, thus the oil recovery.
- The nanoparticle-surfactant flooding presented the highest oil recovery.
- The simultaneous use of nanoparticles and surfactant reduced viscous fingering effect.
- The nanoparticle-surfactant solution modified the wettability of substrates of microfluidic devices.

Declaration of interests

The authors declare that they have no known competing financial interests or personal relationships that could have appeared to influence the work reported in this paper.

The authors declare the following financial interests/personal relationships which may be considered as potential competing interests:

Stefania Betancur
Corresponding author

Journal Pre-proof